THE JOURNAL OF BIOLOGICAL CHEMISTRY VOL. 281, NO. 22, pp. 15370–15375, June 2, 2006

Architecture of Active Mammalian Respiratory Chain Supercomplexes*

Received for publication, February 16, 2006, Published, JBC Papers in Press, March 20, 2006, DOI 10.1074/jbc.M513525200

Eva Schäfer[‡], Holger Seelert[‡], Nicole H. Reifschneider[‡], Frank Krause[‡], Norbert A. Dencher[‡], and Janet Vonck[§1]

From the [‡]Department of Chemistry, Physical Biochemistry, Darmstadt University of Technology, Petersenstrasse 22, D-64287 Darmstadt, Germany and the [§]Department of Structural Biology, Max-Planck-Institute of Biophysics, Max-von-Laue-Strasse 3, D-60438 Frankfurt am Main, Germany

In the inner mitochondrial membrane, the respiratory chain complexes generate an electrochemical proton gradient, which is utilized to synthesize most of the cellular ATP. According to an increasing number of biochemical studies, these complexes are assembled into supercomplexes. However, little is known about the architecture of the proposed multicomplex assemblies. Here, we report the electron microscopic characterization of the two respiratory chain supercomplexes I_1III_2 and $I_1III_2IV_1$ in bovine heart mitochondria, which are also two major supercomplexes in human mitochondria. After purification and demonstration of enzymatic activity, their structures in projection were determined by single particle image analysis. A difference map between the supercomplexes I_1III_2 and $I_1III_2IV_1$ closely fits the x-ray structure of monomeric complex IV and shows its location in the assembly. By comparing different views of supercomplex $I_1III_2IV_1$, the location and mutual arrangement of complex I and the complex III dimer are discussed. Detailed knowledge of the architecture of the active supercomplexes is a prerequisite for a deeper understanding of energy conversion by mitochondria in mammals.

All living organisms use a series of integral membrane protein complexes for energy conversion and ATP synthesis. In eukaryotes, electrons are transported by the respiratory chain, starting from NADH via complex I (NADH:ubiquinone oxidoreductase) or from succinate via complex II (succinate:ubiquinone oxidoreductase), the membrane integral electron carrier ubiquinol, complex III (ubiquinol:cytochrome *c* oxidoreductase), the peripheral electron carrier cytochrome *c*, and complex IV (cytochrome *c* oxidase) to the terminal acceptor molecular oxygen (1). The electron transport chain generates a proton gradient across the inner mitochondrial membrane, which is used by complex V (F_OF_1-ATP synthase) to synthesize ATP. In the last decade, structures of the individual respiratory chain complexes from various organisms have been determined. Atomic models exist for bovine heart mitochondrial complex III (2) and IV (3). A high resolution structure of complex I is not yet available, but electron microscopy indicates that it is L-shaped in all organisms investigated, and a 2.2-nm resolution map from cryoelectron microscopy exists for the bovine heart complex I (4).

Two alternative models for the arrangement of the respiratory chain complexes in the membrane have been proposed. According to the currently favored random collision model (5), all components of the respiratory chain diffuse individually in the membrane, and electron transfer depends on the random, transient encounter of the individual protein complexes and the smaller electron carriers. In the solid state model (6) proposed 50 years ago, the substrate is channeled directly from one enzyme to the next. Recently isolated stoichiometric assemblies, so-called supercomplexes, support this model. Respiratory supercomplexes of different compositions have been described in bacteria (*e.g. Paracoccus denitrificans* (7)) and in mitochondria from *Saccharomyces cerevisiae* (8, 9), other fungi (10), higher plants (11–13), and mammals (8, 14–16) by means of blue native polyacrylamide gel electrophoresis (BN-PAGE),[2] gel filtration and immunoprecipitation. In these studies, supercomplexes of various stoichiometries have been detected, such as assemblies of monomeric complex I (I_1), dimeric complex III (III_2), and complex IV in various copy numbers (IV_x). A crucial function of these respiratory supercomplexes may be the stabilization of the individual complexes (7, 10, 15, 17, 18). Kinetic evidence by inhibitor-titration studies in bovine heart mitochondria is consistent with both models for the arrangement of the respiratory chain complexes and suggests their coexistence (19).

Recently, an electron projection map of a plant supercomplex consisting of only complex I and dimeric complex III (III_2) has been presented for *Arabidopsis thaliana* (20). But so far, the supramolecular architecture of a stoichiometrically defined supercomplex comprising all three complexes (I, III, and IV) has not been determined. By BN-PAGE analysis, the most abundant supercomplexes in bovine heart mitochondria are a supercomplex consisting of complex I and dimeric III and another supercomplex containing complexes I and dimeric III and IV with molecular masses of ~1,500 kDa and 1,700 kDa, respectively (8, 14). By electron microscopy, we could image both supercomplexes from bovine heart mitochondria and localized complex IV unambiguously in the larger assembly.

EXPERIMENTAL PROCEDURES

Bovine Heart Mitochondria Preparation and Supercomplex Isolation—Bovine heart mitochondria were isolated (16, 21), frozen in liquid nitrogen, and stored at −80 °C. Solubilization with 1% (w/v) digitonin (Calbiochem, high purity) was done according to Refs. 8, 10, 13, and 16 in buffer containing 150 mM KOAc, 30 mM HEPES, 10% (w/v) glycerol, 0.5 mM Pefabloc^{TM} SC, pH 7.4, at 4 °C but at a ratio of 28 g of detergent/1 g of protein. To the digitonin extract, sample buffer was added containing 5% (w/v) Coomassie G-250, 500 mM ϵ-aminocaproic acid, 50 mM bis-tris, pH 7.0, to obtain a detergent-to-dye ratio of 4 (w/w).

BN-PAGE was performed with linear gradient gels of a polyacrylamide concentration (T) gradient of 3–13 or 3–5%, overlaid with 3%

* This work was supported by the Deutsche Forschungsgemeinschaft (SFB 472) (to N. A. D., H. S., and W. Kühlbrandt) and by the European Union (MiMage) (to N. A. D.). The costs of publication of this article were defrayed in part by the payment of page charges. This article must therefore be hereby marked "*advertisement*" in accordance with 18 U.S.C. Section 1734 solely to indicate this fact.

[1] To whom correspondence should be addressed: Dept. of Structural Biology, Max-Planck-Institute of Biophysics, Max-von-Laue-Strasse 3, D-60438 Frankfurt am Main, Germany. Tel.: 49-69-6303-3004; Fax: 49-69-6303-3002; E-mail: janet.vonck@mpibp-frankfurt.mpg.de.

[2] The abbreviations used are: BN-PAGE, blue native polyacrylamide gel electrophoresis; bis-tris, 2-[bis(2-hydroxyethyl)amino]-2-(hydroxymethyl)propane-1,3-diol.

stacking gels using buffers with 25 mM imidazole, 500 mM ϵ-aminocaproic acid, 0–20% (w/v) glycerol, pH 7.0, based on Ref. 22. Gel electrophoresis was performed in buffer containing 7.5 mM imidazole, 50 mM tricine, 0.02–0.002% (w/v) Coomassie G-250, pH 7.0 (cathode), and 25 mM imidazole, pH 7.0 (anode).

Protein bands were cut out of the gel and electroeluted in buffer (25 mM tricine, 7.5 mM bis-tris, 25 mM ϵ-aminocaproic acid, pH 7.0) at 4 °C, 75 V, and 2 mA for at least 12 h according to a modified version of Refs. 23 and 24. Afterward, 0.1% (w/v) digitonin was added to prevent protein aggregation.

Matrix-assisted Laser Desorption Ionization-Mass Spectrometry (MALDI-MS)—For MALDI-MS analysis, proteins were separated by SDS-PAGE on a 14% polyacrylamide gel at room temperature and silver-stained. Protein bands were cut out, subjected to in-gel trypsinization, and identified by MALDI time-of-flight mass spectrometry (Applied Biosystems Voyager DE PRO) as described previously (25).

Enzymatic Analysis—NADH dehydrogenase activity of complex I was determined by in-gel formazan precipitation in 100 mM Tris, 768 mM glycine, 0.04% (w/v) 4-nitro blue tetrazolium chloride, 100 μM β-NADH, pH 7.4, according to a modified version of Refs. 10 and 26. The cytochrome *c* oxidase activity of complex IV was visualized by precipitation of 3,3′-diaminobenzidine oxides and indamine polymers in test buffer containing 50 mM sodium phosphate, 0.5 mg/ml 3,3′-diaminobenzidine-tetrahydrochloride, 0.5 mg/ml cytochrome *c* (horse heart), 20 units/ml catalase, and 75 mg/ml sucrose, pH 7.4 (10, 26, 27, 28). Spectrophotometric activity assays of complexes I and III were performed by a procedure modified from Ref. 8 at 20 °C in 150 mM NaCl, 75 mM imidazole, 200 μM β-NADH, 750 μM decylubiquinone, pH 7.4, but with 0.1% (w/v) digitonin. NADH:ubiquinol reductase activity of complex I was measured by the rotenone (50 μM)-sensitive oxidation of NADH (200 μM; ϵ 6.2 $mM^{-1}\cdot cm^{-1}$) at a wavelength of 340 nm. The cytochrome *c* reductase activity of complex III was determined by the antimycin (5 μM)-sensitive cytochrome *c* reduction (70 μM; ϵ 21.1 $mM^{-1}\cdot cm^{-1}$) at a wavelength of 550 nm. 10 mM KCN was added to inhibit cytochrome *c* oxidation by complex IV. To eliminate buffer-dependent effects during the measurements, the test buffer was incubated without protein, and the absorptions were observed. For the actual tests, the buffers with supercomplexes and substrates were observed at the given wavelengths (340 or 550 nm) for 1–3 min. The absorptions decreased linearly, and the decrease/time unit was determined. Afterward, the inhibitors rotenone or antimycin, respectively, were added. The decrease in absorption with the inhibitor was less than that without and was subtracted from the absorption before inhibition to determine the protein-dependent absorption change. All tests were performed three times, and the S.D. was determined.

Electron Microscopy and Single Particle Analysis—The supercomplex samples were negatively stained with 1% (w/v) uranyl acetate, pH ~4. Negative staining with 2% (w/v) ammonium molybdate, pH 6.9, was also carried out and showed equivalent results. Electron micrographs were collected using a Philips CM120 at 120 kV under low dose conditions at a magnification of 45,000× on Kodak SO-163 electron image film. The negatives were checked by optical diffraction for correct defocus and lack of drift and astigmatism and digitized on a PhotoScan scanner (Z/I Imaging, Aalen, Germany) at a pixel size of 7 μm, corresponding to 1.56 Å on the specimen. Subsequently, adjacent pixels were averaged to yield a pixel size of 4.67 Å. The images were processed using Imagic V (Image Science Software GmbH, Berlin, Germany).

RESULTS

To structurally characterize the supercomplexes, bovine heart mitochondria were solubilized with 1% (w/v) digitonin at a ratio of 28 g of digitonin/1 g of protein. Afterward, the solubilizate was separated by BN-PAGE. The protein pattern of respiratory chain complexes resembles that in previous reports (8, 14). It shows the individual complexes I–V, as well as two prominent supercomplex bands, namely I_1III_2 (consisting of one complex I and a dimer of complex III; 1,500 kDa) and $I_1III_2IV_1$ (with one additional complex IV; 1,700 kDa) and some minor supercomplex bands of higher molecular masses (Fig. 1, *a* and *b*). Solubilization was performed at a detergent-to-protein ratio far above the 2–4 g of digitonin/1 g of protein needed for quantitative extraction of the respiratory chain complexes (8, 16). This was done to obtain I_1III_2 and $I_1III_2IV_1$ as the two predominant supercomplex species (Fig. 1, *a* and *b*) while minimizing the amounts of complex V dimers, which because of their comparable mass (~1,500 kDa) would comigrate with I_1III_2. In addition, sharper protein bands were obtained. The employed detergent-to-protein ratio thus facilitated the isolation of the supercomplexes I_1III_2 and $I_1III_2IV_1$.

For biochemical and structural characterization, supercomplexes I_1III_2 and $I_1III_2IV_1$ were excised from the gel and electroeluted. The integrity of the purified supercomplexes was verified by an additional BN-PAGE (Fig. 1*c*) to detect supercomplex fragments, which might arise during electroelution. Supercomplex $I_1III_2IV_1$ remained intact

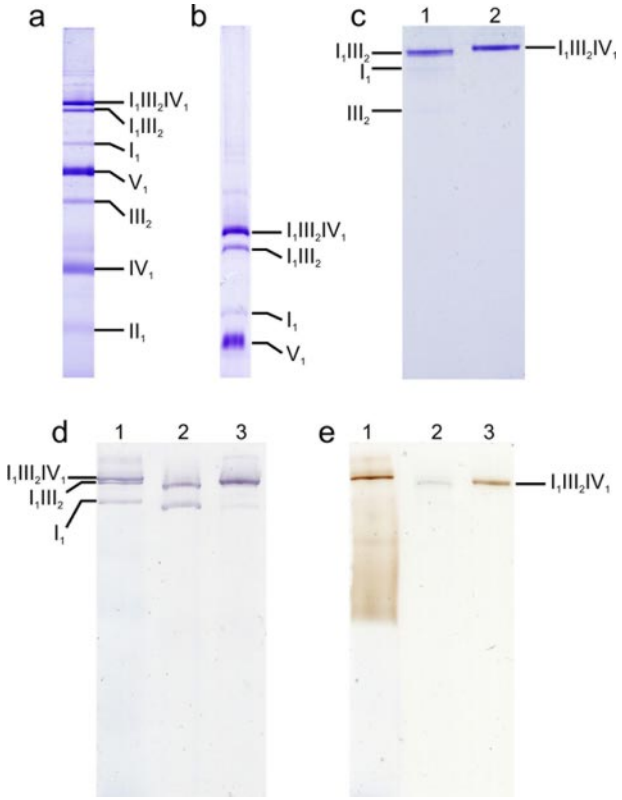

FIGURE 1. **Isolation and activity assay of supercomplexes I_1III_2 and $I_1III_2IV_1$.** *a*, BN-PAGE (polyacrylamide concentration gradient T, 3–13%) of solubilized bovine heart mitochondria. *b*, BN-PAGE (T, 3–5%) of solubilized bovine heart mitochondria. Both supercomplex bands were in close proximity in a BN-PAGE (T, 3–13%). The separation was improved on a BN-PAGE with T at 3–5%. *c*, BN-PAGE (T, 3–13%) of isolated supercomplexes I_1III_2 and $I_1III_2IV_1$. Supercomplex $I_1III_2IV_1$ (*lane 2*) is intact after electroelution, but the supercomplex I_1III_2 sample (*lane 1*) shows two additional very weak bands of I and III_2. The BN gels in *a–c* were Coomassie R-250-stained. *d*, NADH dehydrogenase activity of complex I. Supercomplexes I_1III_2 and $I_1III_2IV_1$, as well as complex I of solubilized bovine heart mitochondria (*lane 1*), isolated I_1III_2, and I (a dissociation product of isolated I_1III_2) (*lane 2*), as well as isolated $I_1III_2IV_1$ (*lane 3*) showed in-gel NADH dehydrogenase activity. *e*, cytochrome *c* oxidase activity of complex IV. Supercomplex $I_1III_2IV_1$ from solubilized bovine heart mitochondria (*lane 1*) and isolated $I_1III_2IV_1$ (*lane 3*) have in-gel cytochrome *c* oxidase activity, whereas I_1III_2 (*lane 2*) lacking complex IV does not. The position of I_1III_2 (in *lane 2*) is indicated by a *faint blue band* resulting from residual Coomassie dye of the BN-PAGE bound to the protein.

TABLE 1

Spectrometric activity measurements of the isolated supercomplex I_1III_2 and $I_1III_2IV_1$

For complex I, the inhibitor (rotenone)-specific NADH:ubiquinol reductase activity, and for complex III, the inhibitor (antimycin)-specific cytochrome *c* reductase activity, is stated.

	Activities	
	NADH:ubiquinol reductase	Cytochrome *c* reductase
	milliunits/mg protein	
Supercomplex I_1III_2	0.13 ± 0.04	0.06 ± 0.02
Supercomplex $I_1III_2IV_1$	0.30 ± 0.11	0.99 ± 0.28

after isolation, whereas in the supercomplex I_1III_2 sample, two minor bands representing complexes I (~1,000 kDa) and III_2 (500 kDa) were present (Fig. 1*c*). The composition of both supercomplexes was confirmed by peptide mass fingerprinting. In total, 20 subunits of the integrated complexes were identified, *e.g.* the 49- and 30-kDa subunits from complex I, core protein II from complex III, and subunit IV from complex IV (data not shown).

The enzymatic activity of each supercomplex component was tested to confirm their functional integrity after isolation. NADH dehydrogenase activity of complex I and cytochrome *c* oxidase activity of complex IV, respectively, were visualized by in-gel activity staining. NADH dehydrogenase activity of complex I was displayed by purple bands resulting from in-gel formazan precipitation (10, 26). The cytochrome *c* oxidase activity of complex IV was determined by the cytochrome *c*-dependent oxidation of 3,3′-diaminobenzidine to brown oxide and indamine precipitates (10, 27, 28). Thus, complex I activity for supercomplexes I_1III_2 and $I_1III_2IV_1$, as well as complex IV activity for supercomplex $I_1III_2IV_1$ in the isolated samples, were demonstrated (Fig. 1, *d* and *e*). Spectrophotometric activity assays using specific inhibitors were employed to assess NADH:ubiquinol reductase activity of complex I and cytochrome *c* reductase activity of complex III in the electroeluted samples. For the latter activity, no in-gel assay exists (28). Under the conditions used, complex I in supercomplex I_1III_2 displayed about half the activity of that in supercomplex $I_1III_2IV_1$ (Table 1). Complex III was active in supercomplex $I_1III_2IV_1$, but supercomplex I_1III_2 showed only minor cytochrome *c* reductase activity (Table 1). In conclusion, both isolated supercomplexes displayed activity, but supercomplex $I_1III_2IV_1$ was significantly more active.

For electron microscopy, the purified supercomplexes I_1III_2 and $I_1III_2IV_1$ were negatively stained with 1% uranyl acetate (Fig. 2). Electron micrographs of both supercomplex samples showed predominantly triangular particles measuring 30–33 nm on the longest side (Fig. 2). In addition, smaller particles were seen in the I_1III_2 sample (Fig. 2*a*). As there are no other proteins present in the sample, the smaller particles might be individual complex III dimer arising from partial disintegration of the supercomplex. This observation is consistent with the minor supercomplex I_1III_2 dissociation seen on BN-PAGE (Fig. 1*c*). Another less frequent view on the micrographs is an L-shaped particle (Fig. 2).

~1,400 triangular particles of supercomplex $I_1III_2IV_1$ were selected for image analysis and subjected to multireference alignment, multivariate statistical analysis, and classification (29). 14% of the selected particles did not align well and were rejected.

All classes displayed asymmetrical triangles, with three sides of different lengths (Fig. 3). Two orientations with a bright stain-excluding density pointing either right or left were present. The view with the density pointing right represented ~80% of the particles (Figs. 3*a* and 4*a*) and the other ~20% (Figs. 3*b* and 4*d*). All classes of the same orientation displayed similar general features with no pronounced differences. It can be concluded that the two views represent the two preferential orientations of the supercomplexes on the carbon support film with opposite sides attached to the film. Apparently, one orientation is preferred over the other.

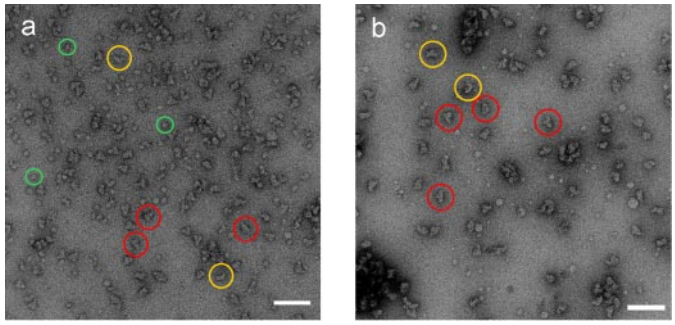

FIGURE 2. **Transmission electron microscopic images of isolated supercomplexes I_1III_2 (a) and I_1 III_2IV_1 (b).** Triangular views are indicated by *red circles* and L-shaped views by *yellow circles*. The *green circles* in *a* indicate particles that might be dimeric complex III arising from the dissociation of supercomplex I_1III_2. Both samples were negatively stained with 1% uranyl acetate. The *scale bars* represent 100 nm.

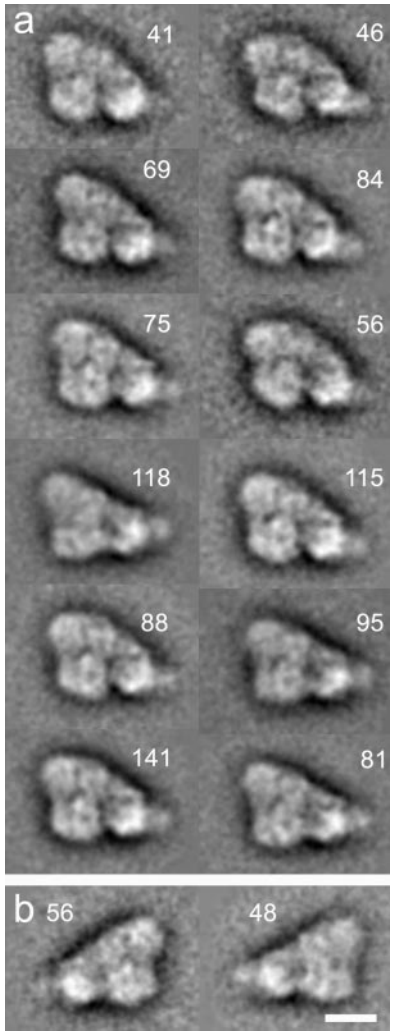

FIGURE 3. **Class averages of supercomplex $I_1III_2IV_1$ triangular views.** *a*, the majority of classes show the same view with the same orientation on the carbon support film. This *top view* shows the supercomplex seen from the intermembrane space (see "Results"). *b*, a minor group of classes represents the opposite orientation, a view from the matrix side. The *numbers* in the *top right* or *left* are the number of particles belonging to that class. The *scale bar* represents 10 nm.

All classes displayed asymmetrical triangles, with three sides of different lengths (Fig. 3). Two orientations with a bright stain-excluding density pointing either right or left were present. The view with the density pointing right represented ~80% of the particles (Figs. 3*a* and 4*a*) and the other ~20% (Figs. 3*b* and 4*d*). All classes of the same orientation displayed similar general features with no pronounced differences. It can be concluded that the two views represent the two preferential orientations of the supercomplexes on the carbon support film with opposite sides attached to the film. Apparently, one orientation is preferred over the other.

Another typical view was observed less frequently than the triangular views (Fig. 2). This was characterized by a bright stain-excluding line of

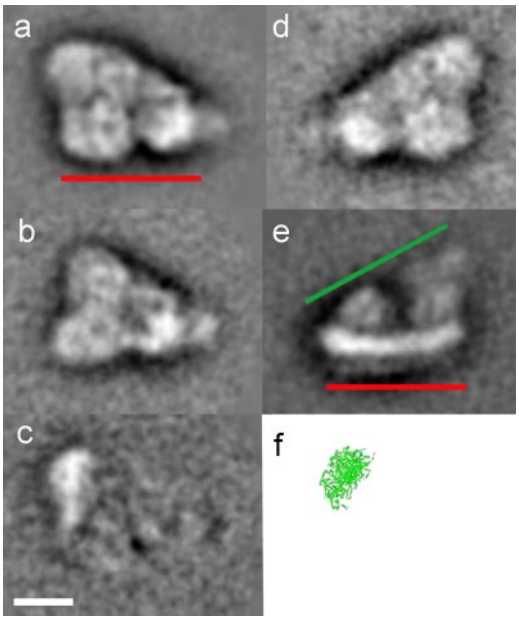

FIGURE 4. **Averaged projection maps of the supercomplexes.** *a*, *top views* (as seen from the intermembrane space) of supercomplex $I_1III_2IV_1$ (average of 228 particles). A resolution of 3.3 and 3.4 nm was determined by Fourier ring correlation (36) according to the 3σ criterion or the 0.5 cutoff criterion, respectively. *b*, supercomplex I_1III_2 *top view* (average of 66 particles). *c*, difference map of $I_1III_2IV_1$ minus I_1III_2. *d*, *top view* (from the matrix space) of $I_1III_2IV_1$. *e*, *side view* of supercomplex $I_1III_2IV_1$ (average of 70 particles). To get the correct side view from a top view (*a*), the carbon film would be on the *bottom* of the *top view* (*red line*). To derive the two top views (*a* and *d*) from the side view (*e*), the film would be on the *bottom* (*red line*) or on the *top* (*green line*) of the side view, respectively. Because the *red* and the *green lines* are not parallel in *e*, the *top views* in *a* and *d* are not mirror images. *f*, *top view* of the bovine complex IV x-ray structure as seen from the intermembrane space (*green*, Protein Data Bank (PDB) accession code 1OCC). The *scale bar* represents 10 nm.

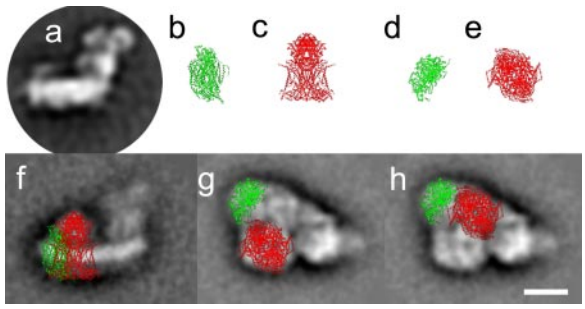

FIGURE 5. **Alternative arrangements of the complexes I and III_2 in supercomplex $I_1III_2IV_1$.** *a*, projection structure of bovine complex I, average of 300 particles (from Ref. 30). Shown are *side views* of x-ray structures of bovine complex IV (*green*, PDB accession code 1OCC) (*b*) and bovine complex III dimer (*red*, PDB accession code 1BGY) (*c*) drawn at the same scale as the projection maps. The x-ray structure of bovine complex IV (*green*) (*d*) and bovine complex III_2 (*red*) (*e*) are both shown as seen from the intermembrane space. *f*, x-ray structures of complexes III_2 and IV superimposed on the projection map of the supercomplex $I_1III_2IV_1$ side view. *g*, (model 1), complexes III_2 and IV superimposed on the supercomplex $I_1III_2IV_1$ top view (as looking from the intermembrane space). Complex III_2 is in the *lower part* of the supercomplex, and the remaining density in the *upper part* is the membrane arm of complex I. The matrix arm is indicated by the *white* stain-depleted *right corner*. Thus complex IV shares a large contact surface with complex I and only a small one with III_2. *h*, (model 2), complex III_2 is in the *upper part* of the supercomplex. The remaining mass in the *lower part* is the membrane arm of complex I. Thus complex IV is sharing a large contact surface with III_2 but makes only little contact with complex I. The *scale bar* represents 10 nm.

~3 nm width. ~300 particles of this view of supercomplex $I_1III_2IV_1$ were selected. After alignment and averaging, the resulting image showed two large protrusions on one side of the bright line, whereas the other surface appeared smooth (Fig. 4*e*).

Based on their known electron microscopic and x-ray structures, the protrusions in this view can be assigned unambiguously to the individual complexes I and III_2. Comparison with a recent negative stain projection map of the bovine heart complex I (Fig. 5*a*) (30) identifies the largest protrusion (Fig. 4*e*, *right*) as the matrix arm of complex I. The membrane domain of complex I in the supercomplex extends along to the smaller protrusion in this view. The bright line around the supercomplex can be interpreted as the transmembrane domains of the protein decorated by detergent and possibly Coomassie stain from the BN-PAGE. Hence, this class represents a side view along the plane of the membrane.

The matrix arm of isolated complex I (Fig. 5*a*) (30) displays a >90° angle with the membrane, whereas this angle is close to 90° in the supercomplex (Figs. 4*e* and 5*f*). This might be due to the different isolation procedures, a different viewing angle, or conformational changes induced by the supercomplex assembly.

The smaller protrusion fits the matrix domains of the complex III dimer (2) (Figs. 4*e* and 5*f*). Complex IV has a much smaller matrix domain (3), which cannot be identified in the present side view. Neither complex I, III_2, nor IV has a noticeable domain exposed to the intermembrane space, which is consistent with the smooth appearance of this surface in the side views.

The asymmetry of the side view (Fig. 4*e*) clearly explains the distinct triangular views (Fig. 4, *a* and *d*), which can be interpreted as views perpendicular to the membrane (top views) from the matrix and intermembrane space side, respectively. Because of the asymmetric nature of the supercomplex, the two top views are not exactly 180° rotated relative to each other and thus do not form mirror images. By comparing the top and side views of supercomplex $I_1III_2IV_1$, the matrix arm of complex I can be identified in the top views as a bright stain-excluding density at the sharpest corner of the triangle (Fig. 4, *a* and *d*). In the side view, the distal domains of the complex I matrix arm extend beyond the membrane arm (Fig. 4*e*). This is visible in the top views as a diffuse extension (Fig. 4; *a*, *b*, and *d*).

To localize complex IV in the $I_1III_2IV_1$ projections, the smaller supercomplex I_1III_2 was compared with the larger one. ~1,400 images were selected and analyzed. The great majority showed triangular views, similar to the $I_1III_2IV_1$ top views but with two sides of approximately the same length (Fig. 4*b*). A difference map of $I_1III_2IV_1$ minus I_1III_2 displays a density of ~13 × 7 nm (Fig. 4*c*) at the side opposite the complex I matrix arm. This density matches closely the projection of a complex IV monomer viewed from the intermembrane space toward the matrix (Figs. 4*f* and 5, *d*, *g*, and *h*). It is worth noting that the complex IV monomer interacts with the other components of the supercomplex (Fig. 5) through the interface, which is the dimer interface in the x-ray structure (3).

In the top views, complex IV and the matrix arm of complex I could be assigned unambiguously. Two densities remain that each would fit the membrane arm of complexes I or III_2 (Fig. 5, *g* and *h*). The top view two-dimensional projections were calculated from the published three-dimensional data (2) of complex III dimer and filtered to 3.0 nm. They were cross-correlated with the two densities in the supercomplex where III_2 might be located. The cross-correlation coefficients for the upper density in the supercomplex and III_2 were ~0.55–0.6, whereas the ones for the lower density with III_2 were ~0.7. Thus complex III_2 viewed from the intermembrane side has a higher similarity with the lower density in the supercomplex top view. However, as the cross-correlation coefficients for the two locations differ only by 10–15%, neither location of I and III_2 in the top view can be ruled out at present (Fig. 5, *g* and *h*).

DISCUSSION

The two respiratory chain supercomplexes I_1III_2 and $I_1III_2IV_1$ from bovine heart mitochondria were isolated in an active state and were

structurally characterized by transmission electron microscopy. Our results show that the two digitonin-solubilized supercomplexes I_1III_2 and $I_1III_2IV_1$ are structurally related to one another, I_1III_2 being a building block of the larger supercomplex $I_1III_2IV_1$.

The structures we found for the two supercomplexes studied confirm their stoichiometries of I_1III_2 and $I_1III_2IV_1$, as deduced from BN-PAGE (8, 14, 16). Mitochondrial complex III forms a dimer in the crystal structures of the bovine (2), chicken (31), and yeast (32) enzymes. The crystal structures suggest that the complex is functional as a dimer, which is supported by data showing that the two monomers differ in their cytochrome *c* binding properties and their ubiquinone reduction sites (33) and that electrons are transferred between equivalent hemes in the two monomers (34). The fact that a complex III dimer is seen in the supercomplexes of both bovine heart (this work) and plant mitochondria (20) strongly supports the existence of a functional dimer for complex III. In addition, our finding of well defined structures for the supercomplexes supports biochemical data showing that complex III dimer is essential for assembly/stability of complex I (7, 10, 15, 17, 18).

Bovine heart complex IV is also dimeric in the crystal structure (3) but is clearly monomeric in the supercomplex (Fig. 4, *c* and *f*). Complex IV is associated with the rest of the supercomplex through the concave face, which is the dimer interface in the x-ray structure. No functional role of complex IV dimerization has been suggested, and our finding of a single copy in the supercomplex suggests a structural rather than a functional role of dimer formation. The crystal dimer contact in the 13-subunit complex IV is not very extensive and is formed by both copies of subunit VIb interacting with each other on the intermembrane space side and by the N terminus of subunit VIa interfacing with subunit III of the other monomer near the matrix interface. Between these contact sites, the two monomers are separated by 8–10 Å, enough space to accommodate lipids. It is conceivable that dimer formation competes with supercomplex formation using the same contact interface. The existence of larger supercomplexes in bovine heart mitochondria, which differ only in the copy number of complex IV from 1 to 4 (8, 14), suggests that the association of complex IV is rather promiscuous. However, the abundance and high stability of $I_1III_2IV_1$ indicates that the contact of complex IV made in this supercomplex is particularly strong. After isolation, $I_1III_2IV_1$ remained intact and active, whereas a minor fraction of I_1III_2 disintegrated into its individual complexes, suggesting a role for complex IV in the stability of the supercomplex.

In the recently published supercomplex I_1III_2 projection map from plant mitochondria (20), the interaction between complexes I and III_2 appears to be different from that in our bovine heart mitochondrial supercomplexes. The bovine supercomplex I_1III_2 is triangular, whereas the corresponding view of the plant supercomplex is V-shaped. Plant and bovine complex I differ considerably in their subunit composition (35), which can explain the structural difference between plant and mammalian supercomplexes.

Based on our structural data, complex IV and the matrix arm of complex I of the respiratory chain supercomplex $I_1III_2IV_1$ were localized unambiguously, as well as complex I and III_2 in the side view (Fig. 5, *f–h*). For the arrangement of complexes I and III_2 in the top views of supercomplex $I_1III_2IV_1$, we present two models, as their location could not be determined unambiguously with the present electron microscope data. In both models, complex IV is at the upper left-hand corner and the matrix arm of complex I at the sharp right-hand corner of the supercomplex $I_1III_2IV_1$ top view from the intermembrane space (Fig. 5, *g* and *h*).

In model 1, complex III_2 is at the lower and the membrane arm of I at the upper part of the top view (Fig. 5*g*). Hence, complex III_2 and IV are attached to complex I but share only a small contact surface. In the alternative model 2, complex III_2 is at the upper part of the top view (Fig. 5*h*) and attached to complexes I and IV, having large interfaces with both. The membrane arm of complex I is at the lower part. Thus, complexes I and IV share only a small contact surface.

In model 1, complex IV is attached to complex I, whereas in model 2, the main contact site of complex IV is to complex III_2. Biochemical data exist that can distinguish between the two models. The small supercomplexes III_2IV_1 and III_2IV_2, as well as I_1IV_1, can be separated from mildly solubilized bovine heart mitochondria (8, 16), indicating that complex IV can bind to both complexes I and III_2. However, mild dissociation of the supercomplex $I_1III_2IV_1$ in a two-dimensional BN-PAGE by 0.03% Triton X-100 as an additive yielded, besides the three individual complexes and undissociated $I_1III_2IV_1$, a significant amount of the smaller supercomplex I_1IV_1 but no III_2IV_1 (8). This biochemical observation, as well as the higher cross-correlation coefficients of complex III_2 with the lower density in the supercomplex, both favor an arrangement of the complexes as proposed in model 1 (Fig. 5*g*), with complex IV attached to complex I.

To determine the location of complex III_2 and the membrane part of complex I unambiguously in the supercomplex, either a three-dimensional map or specific antibody labeling of the complexes is required. Both approaches are under way.

Our data confirm the stoichiometries of I_1III_2 and $I_1III_2IV_1$ that were proposed based on biochemical data (8, 14, 16). In addition these data suggest that the supercomplex $I_1III_2IV_1$ is a major physiological module of the respiratory chain in mammalian mitochondria.

Acknowledgments—We thank Mihnea Bostina, Ulrich Brandt, and Volker Zickermann for the bovine complex I projection, Deryck Mills and Remco Wouts for help with electron microscopy and computing, David Wright for advice in determining the cross-correlation coefficients, and Werner Kühlbrandt for support and discussions, as well as critical reading of the manuscript.

REFERENCES

1. Hatefi, Y. (1985) *Annu. Rev. Biochem.* **54,** 1015–1069
2. Iwata, S., Lee, J. W., Okada, K., Lee, J. K., Iwata, M., Rasmussen, B., Link, T. A., Ramaswamy, S., and Jap, B. K. (1998) *Science* **281,** 64–71
3. Tsukihara, T., Aoyama, H., Yamashita, E., Tomizaki, T., Yamaguchi, H., Shinzawa-Itoh, K., Nakashima, R., Yaono, R., and Yoshikawa, S. (1996) *Science* **272,** 1136–1144
4. Grigorieff, N. (1998) *J. Mol. Biol.* **277,** 1033–1046
5. Hackenbrock, C. R., Chazotte, B., and Gupte, S. S. (1986) *J. Bioenerg. Biomembr.* **18,** 331–368
6. Chance, B., and Williams, G. R. (1955) *Nature* **176,** 250–254
7. Stroh, A., Anderka, O., Pfeiffer, K., Yagi, T., Finel, M., Ludwig, B., and Schägger, H. (2004) *J. Biol. Chem.* **279,** 5000–5007
8. Schägger, H., and Pfeiffer, K. (2000) *EMBO J.* **19,** 1777–1783
9. Cruciat, C. M., Brunner, S., Baumann, F., Neupert, W., and Stuart, R. A. (2000) *J. Biol. Chem.* **275,** 18093–18098
10. Krause, F., Scheckhuber, C. Q., Werner, A., Rexroth, S., Reifschneider, N. H., Dencher, N. A., and Osiewacz, H. D. (2004) *J. Biol. Chem.* **279,** 26453–26461
11. Eubel, H., Jänsch, L., and Braun, H. P. (2003) *Plant Physiol.* **133,** 274–286
12. Eubel, H., Heinemeyer, J., and Braun, H. P. (2004) *Plant Physiol.* **134,** 1450–1459
13. Krause, F., Reifschneider, N. H., Vocke, D., Seelert, H., Rexroth, S., and Dencher, N. A. (2004) *J. Biol. Chem.* **279,** 48369–48375
14. Schägger, H., and Pfeiffer, K. (2001) *J. Biol. Chem.* **276,** 37861–37867
15. Schägger, H., de Coo, R., Bauer, M. F., Hofmann, S., Godinot, C., and Brandt, U. (2004) *J. Biol. Chem.* **279,** 36349–36353
16. Krause, F., Reifschneider, N. H., Goto, S., and Dencher, N. A. (2005) *Biochem. Biophys. Res. Commun.* **329,** 583–590
17. Schägger, H. (2002) *Biochim. Biophys. Acta* **1555,** 154–159
18. Acin-Perez, R., Bayona-Bafaluy, M. P., Fernandez-Silva, P., Moreno-Loshuertos, R., Perez-Martos, A., Bruno, C., Moraes, C. T., and Enriquez, J. A. (2004) *Mol. Cell* **13,** 805–815
19. Bianchi, C., Genova, M. L., Parenti Castelli, G., and Lenaz, G. (2004) *J. Biol. Chem.*

279, 36562–36569
20. Dudkina, N. V., Eubel, H., Keegstra, W., Boekema, E. J., and Braun, H. P. (2005) *Proc. Natl. Acad. Sci. U. S. A.* **102,** 3225–3229
21. Smith, A. L. (1967) *Methods Enzymol.* **10,** 81–86
22. Schägger, H. (2001) *Methods Cell Biol.* **65,** 231–244
23. Schägger, H., and von Jagow, G. (1991) *Anal. Biochem.* **199,** 223–231
24. Poetsch, A., Neff, D., Seelert, H., Schägger, H., and Dencher, N. A. (2000) *Biochim. Biophys. Acta* **1466,** 339–349
25. Rexroth, S., Meyer zu Tittingdorf, J. M. W., Krause, F., Dencher, N. A., and Seelert, H. (2003) *Electrophoresis* **24,** 2814–2823
26. Grandier-Vazeille, X., and Guérin, M. (1996) *Anal. Biochem.* **242,** 248–254
27. Angermüller, S., and Fahimi, H. D. (1981) *Histochemistry* **71,** 33–44
28. Zerbetto, E., Vergani, L., and Dabbeni-Sala, F. (1997) *Electrophoresis* **18,** 2059–2064
29. van Heel, M., Harauz, G., Orlova, E. V., Schmidt, R., and Schatz, M. (1996) *J. Struct. Biol.* **116,** 17–24
30. Bostina, M. (2004) *Determination of the Structure of Complex I of Yarrowia lipolytica by Single Particle Analysis* Ph.D. thesis, Physics Department, Johann Wolfgang Goethe University, Frankfurt, Germany
31. Zhang, Z. L., Huang, L.-S., Shulmeister, V. M., Chi, Y.-I., Kim, K. K., Huang, L.-W., Crofts, A. R., Berry, E. A., and Kim, S.-H. (1998) *Nature* **392,** 677–684
32. Hunte, C., Koepke, J., Lange, C., Robmanith, T., and Michel, H. (2000) *Structure* (*Camb.*) **8,** 669–684
33. Lange, C., and Hunte, C. (2002) *Proc. Natl. Acad. Sci. U. S. A.* **99,** 2800–2805
34. Gong, X., Yu, L., Xia, D., and Yu, C.-A. (2005) *J. Biol. Chem.* **280,** 9251–9257
35. Gabaldon, T., Rainey, D., and Huynen, M. A. (2005) *J. Mol. Biol.* **348,** 857–870
36. van Heel, M. (1987) *Ultramicroscopy* **21,** 95–100

Architecture of Active Mammalian Respiratory Chain Supercomplexes

Eva Schäfer, Holger Seelert, Nicole H. Reifschneider, Frank Krause, Norbert A. Dencher and Janet Vonck

J. Biol. Chem. 2006, 281:15370-15375.
doi: 10.1074/jbc.M513525200 originally published online March 20, 2006
